Research in Astron. Astrophys. **2010** Vol. **10** No. **1**, 39 – 46
http://www.raa-journal.org *http://www.iop.org/journals/raa*

***R**esearch in*
***A**stronomy and*
***A**strophysics*

A possible explanation for the electron/positron excess of ATIC/PAMELA

Rui-Zhi Yang, Jin Chang and Jian Wu

Purple Mountain Observatory, Chinese Academy of Sciences, Nanjing 210008, China;
bixian85@mail.ustc.edu.cn

Received 2009 June 3; accepted 2009 October 11

Abstract Results from PAMELA and ATIC indicate that the Kaluza-Klein type dark matter particles could be the annihilation source of the observed excess of electrons and positrons. Assuming the existence of a nearby black hole with 10 000–100 000 solar masses and a point source boost algorithm, we apply the standard propagation model and find that the results fit the data well.

Key words: dark matter — black hole physics — cosmic rays

1 INTRODUCTION

The standard cosmological model points out that cold dark matter (DM) comprises about 1/4 of the total energy density of the universe. Standard Model (SM) particles cannot concurrently explain the electron/positron excess and the unobserved excess of gamma/radio photons except that the DM density profile is much shallower than the Navarro, Frenk & White (NFW) profile at galactocentric radii below 100 pc. New non-baryonic particles from the extended SM are proposed as candidates for this cold DM. Among these extended models, supersymmetric extension lists particles with masses up to the electro-weak scale as DM candidates, such as the Lightest Kaluza-Klein Particle (LKP) from the Universal Extra Dimension (UED) model and the Lightest Supersymmetry Particle (LSP) from Supersymmetry (SUSY). Their stability is guaranteed by KK parity and R-parity respectively. Direct and indirect observations are the two methods of detecting DM. This paper is related to the indirect observation of DM, i.e., the search for SM particles which are the annihilation products of DM particles. These annihilation products propagate through the galactic halo before they reach the earth. Their energy spectrum contains important information on the DM particles. Recent results from both ATIC and PAMELA show an electron/positron excess in the energy ranges 10–60 GeV and 100–800 GeV, respectively, which could be evidence of the existence of DM.

2 HALO PROPAGATION MODEL AND BACKGROUND

Positron/electron propagation in the galaxy can be described by the following equation within the cosmic ray model (Delahaye et al. 2008)

$$\frac{\partial \varphi}{\partial t} - \nabla[K(\boldsymbol{x}, E)\nabla\varphi] - \frac{\partial}{\partial E}[b(E)\varphi] = q(\boldsymbol{x}, E), \tag{1}$$

where φ is the positron/electron flux, q is the source function, $q(\boldsymbol{x}, E) = \eta\langle\sigma v\rangle\left(\frac{\rho(\boldsymbol{x})}{m_\chi}\right)^2 f(E)$, and ρ is the density of the DM particles. In this case, η is a parameter relevant to DM particles, which is 1/4 for Dirac particles and 1/2 for Majorana particles. Moreover, $\langle\sigma v\rangle$ is constrained by results from WMAP observations and set as $2.1 \times 10^{-26}\,\mathrm{cm^3\ s^{-1}}$. Also K is a diffusion coefficient that has the form of $K(\boldsymbol{x}, E) = K_0(E/1\,\mathrm{GeV})^\delta$ and b is the continuous energy loss. The halo is treated as a cylinder with Dirichlet boundary conditions. The dark matter distribution in it selects a certain density function such as NFW or Moore (see Table 1). Generally, the density profile has the form

$$\rho(r) = \rho_0\left(\frac{r_0}{r}\right)^\gamma\left(\frac{1+\frac{r_0}{r_s}}{1+\frac{r}{r_s}}\right)^{(\beta-\gamma)/\alpha}, \tag{2}$$

where ρ_0 is the local density. WMAP data show $\rho_0 = 0.3\,\mathrm{GeV\ cm^{-3}}$ and r_0 is the distance to the galactic center, i.e., 8.5 kpc.

Table 1 Dark Matter Distribution Profiles in the Milky Way

Halo model	α	β	γ	r_s(kpc)
Cored isothermal	2	2	0	5
NFW	1	3	1	20
Moore	1.5	3	1.3	30

Halo parameters are constrained by Boron/Carbon observations (see Table 2) (Maurin et al. 2001). The diffusion function is factorized using the Green or Bessel method (Delahaye et al. 2008). The positron flux at the earth is obtained by integrating over the whole halo.

Table 2 Acceptable K_0 Range for Different δ Constrained by the B/C Ratio

δ	K_0 ($\mathrm{kpc^2\ Myr^{-1}}$)
0.85	0.0015–0.0035
0.7	0.003–0.03
0.6	0.0045–0.06
0.5	0.01–0.075
0.46	0.056–0.1

The electron/positron backgrounds are depicted by the fitted results of Strong 98 (Moskalenko & Strong 1998) as,

$$\frac{d\phi}{dE}_{\mathrm{prim},e^-} = \frac{0.16E^{-1.1}}{1+16E^{0.9}+3.2E^{2.15}}\ \mathrm{GeV^{-1}\ cm^{-2}\ sr^{-1}\ s^{-1}}, \tag{3}$$

$$\frac{d\phi}{dE}_{\mathrm{sec},e^-} = \frac{0.70E^{0.7}}{1+110E^{1.5}+600E^{2.9}+580E^{4.2}}\ \mathrm{GeV^{-1}\ cm^{-2}\ sr^{-1}\ s^{-1}}, \tag{4}$$

$$\frac{d\phi}{dE}_{\mathrm{sec},e^+} = \frac{4.5E^{0.7}}{1+650E^{2.3}+1500E^{4.2}}\ \mathrm{GeV^{-1}\ cm^{-2}\ sr^{-1}\ s^{-1}}, \tag{5}$$

which has an uncertainty of about 10%.

3 INTERMEDIATE MASS BLACK HOLE AS A POSSIBLE BOOST

An intermediate mass black hole (IMBH) with 20 to $10^6\,M_\odot$ could be a possible boost (Fornasa & Bertone 2008; Bertone et al. 2005). It is included in the sub-halo structure and can effectively

increase the power index of the density distribution, which in turn increases the DM density around it. As the source function is proportional to density squared, this will greatly promote the positron flux. There are two models of an IMBH in earlier papers (Bertone et al. 2005) that give numerical simulation results for the mass distribution. We take into consideration the second model within which the black hole is created by gravitational collapse of a protogalactic pressure-supported disk structure at the center of the gas cloud in our work. The black hole has a mass range of up to $10^6\,M_\odot$.

For simplicity, we treat the source of DM near the black hole as a point source. This means that the flux can be derived by calculating the Green's function of the position. According to the source definition, we define $Q = \left(\frac{\rho}{\rho_{\rm local}}\right)^2 \cdot V$ as the intensity of the point source. Then, the Q value of IMBH can be evaluated.

We place the black hole at the center of a DM sub halo. An NFW type density function is set for the sub-halo at the IMBH and $r_{\rm s}$ is selected to be 200 pc. The gravitational effective distance $r_{\rm h}$ of the black hole is defined as the point at which the gravitational potential of the particle is equal to its kinetic energy,

$$r_{\rm h} = \frac{GM}{\sigma^2} = 11{\rm pc}\left(\frac{M}{10^8 M_\odot}\right)\left(\frac{\sigma}{200{\rm km\ s^{-1}}}\right)^{-2}, \tag{6}$$

where σ is the velocity dispersion and M is the black hole mass. However, for the IMBH, σ depends on the radius. Hence, we take another definition of (Bertone et al. 2005):

$$M(r < r_{\rm h}) = 2M_{\rm BH}. \tag{7}$$

For a black hole with $10^4 - 10^5\,M_\odot$, $r_{\rm h}$ would be of the order of 1 pc. Simulation shows that a spike occurs at about $0.2\,r_{\rm h}$ (Fornasa & Bertone 2008), i.e., the density becomes steeper with respect to the radius from that point. For the NFW model, $\rho \propto r^{-2.33}$ (Fornasa & Bertone 2008); above this radius a power of –1 is seen instead. Beyond $r_{\rm s}$, in the NFW model, the density is proportional to the inverse of the distance cubed. The distance between the sub-halo and the solar system is set to be 1 kpc for the following calculations. So, at a distance $r_{\rm s}$ from the black hole, the DM density should be $(1000/200)^3 = 125$ times the solar system DM density. Between $0.2\,r_{\rm h}$ and $r_{\rm s}$, the index of the density profile is –1. Then at $0.2\,r_{\rm h}$, the DM density should be $200/0.2\,r_{\rm h} = 200/0.2 = 1000$ times the density at $r_{\rm s}$. So the density at $0.2\,r_{\rm h}$, inside which the density becomes steeper, becomes about 100 000 times the density of the DM particles in the solar system. Q can be calculated as,

$$Q = \int_{r_{\rm cut}}^{0.1} 10^{10}\left(\frac{0.1}{r}\right)^{4.67} 4\pi r^2 dr({\rm pc}^3), \tag{8}$$

where $r_{\rm cut}$ is a high density cutoff at which the density will not increase any further. It should be the bigger one between the minimum radius of the stable orbit around the black hole and the radius at which the DM density reaches a maximum in the density-radius function. The DM density can be evaluated by requiring that the density should not obviously decrease due to its annihilation, shown as $\langle\sigma v\rangle \cdot t \cdot N < 1$, where n is numeric density and T is the time scale assumed to be 10^{10} yr. The maximum calculated value of n is 10^9, which is about 10^{12} times the density of the solar system. The corresponding radius is about 10^{-4} pc, much larger than the stable radius which is about several times the Schwarzschild radius. Thus, $r_{\rm cut}$ is set to be 10^{-4} pc. Q can be of the order of $10^4\,{\rm kpc}^3$ after integration.

4 DATA FROM PAMELA AND ATIC, AND AN EXPLANATION

4.1 LKP as the DM Particle

The positron excess in the 10–60 GeV energy range from the PAMELA (Adriani et al. 2009a) experiment introduces an important difficulty to the simple MSSM model. The Majorana property of LSP

greatly suppresses its direct annihilation into leptons. Leptons from LSP are secondary annihilation products of W bosons, meaning that the spectrum must be soft which will not result in the excess at this high energy. In the mean time, anti-proton data fit the standard cosmos model well. As LSP can also annihilate into anti-protons, the lack of excess in anti-protons again causes difficulty with the LSP model. In contrast, LKP can overcome this problem by direct annihilation into leptons with a hard positron spectrum.

Based upon the upper estimate, Q is selected to be $3 \times 10^4\,\mathrm{kpc}^3$ and KK is picked as the DM particle. Because the point source is slightly distant from the solar system, the continuum energy loss may induce the energy peak observed in ATIC to be slightly lower than the DM particle mass. So, we choose the DM particle mass to be 800 GeV. The IMBH is assumed to be 1 kpc from the solar system. The halo parameter is set to $K_0 = 0.0016$ and $\delta = 0.85$. The output positron/electron ratio is plotted in Figure 1(a). The results fit the PAMELA data in the energy range 10−60 GeV well. The small deviation from the experimental data in the 10−20 GeV energy range could result from the uncertainty of the background spectrum that we choose. The uncertainty due to diffusion is considered. We choose the other two typical combinations of the diffusion parameter, $K_0 = 0.0112$ and $\delta = 0.7$, $K_0 = 0.006$ and $\delta = 0.55$, and use the same settings for the source. The results are also shown in Figure 1(b) and (c), respectively.

Hence, the uncertainty due to diffusion is quite large and further study of the cosmic ray data will give a better constraint. We can also assume that the distance is slightly longer or shorter. However, the DM particle mass should also be different because different distances cause the energy loss to be stronger or weaker. We assume the distance to be 1.2 kpc and mass to be 1 TeV, and the distance to be 0.8 kpc and mass to be 700 GeV and we obtain Figure 1(d) and (e), respectively. To fit the PAMELA data, we choose a different Q value for these two situations, 2×10^4 for the 700 GeV and 6×10^4 for the 1000 GeV.

However, sources much closer or further away cannot be used to interpret the data very well. This can be explained by the following analysis. Because KK particles can annihilate directly into leptons, including positrons, if the source is closer, then the positron flux will be concentrated at an even higher energy range, resulting in no obvious excess between 10 and 60 GeV. On the other hand, if it is further away, the exponential form of the Green's function means that the flux attenuates quickly, thus requiring larger Q. However, a Q value with order higher than $10^4\,\mathrm{kpc}^3$ is difficult to explain with the IMBH model. So, an IMBH 1 kpc away from the solar system could be a possible explanation for the PAMELA signals.

4.2 The Problem of Anti-proton

The anti-proton data from PAMELA (Adriani et al. 2009b) show no excess with respect to traditional theory, thus setting limits on DM models. For a KK particle, anti-protons come from its direct annihilation into a quark and anti-quark pair which in turn hadronize through the string fragmentation process. Both the quark and anti-quark have a single energy, the sum of which is the mass of the two DM particles. In our calculation, we choose the LKP model (Hooper & Profumo 2007) where $B^{(1)}$ is the LKP particle and the annihilation branching ratio into quark pairs is 0.35. For simplicity, we let them annihilate to u-$\bar{\mathrm{u}}$, c-$\bar{\mathrm{c}}$ and t$\bar{\mathrm{t}}$ pairs with the same branching ratio and neglect the annihilation to other pairs. In fact, the annihilation branching ratio to other flavors is quite small, so our simplification makes sense. The detailed branching ratio for annihilation is shown in table 2 of Hooper & Profumo (2007). This process is simulated with the PYTHIA package. The anti-proton propagation in the galaxy is somewhat different from that of the positron (Barrau et al. 2005; Donato et al. 2009). Continuous energy loss processes such as synchrotron and inverse Compton scattering (IC) can be neglected due to the anti-proton's much higher mass while its annihilation with hydrogen atoms in the galaxy should be counted. At the same time, the Galaxy's outflow convective current has to be considered. As the solar system could be taken as sitting on the disk, the convective current will

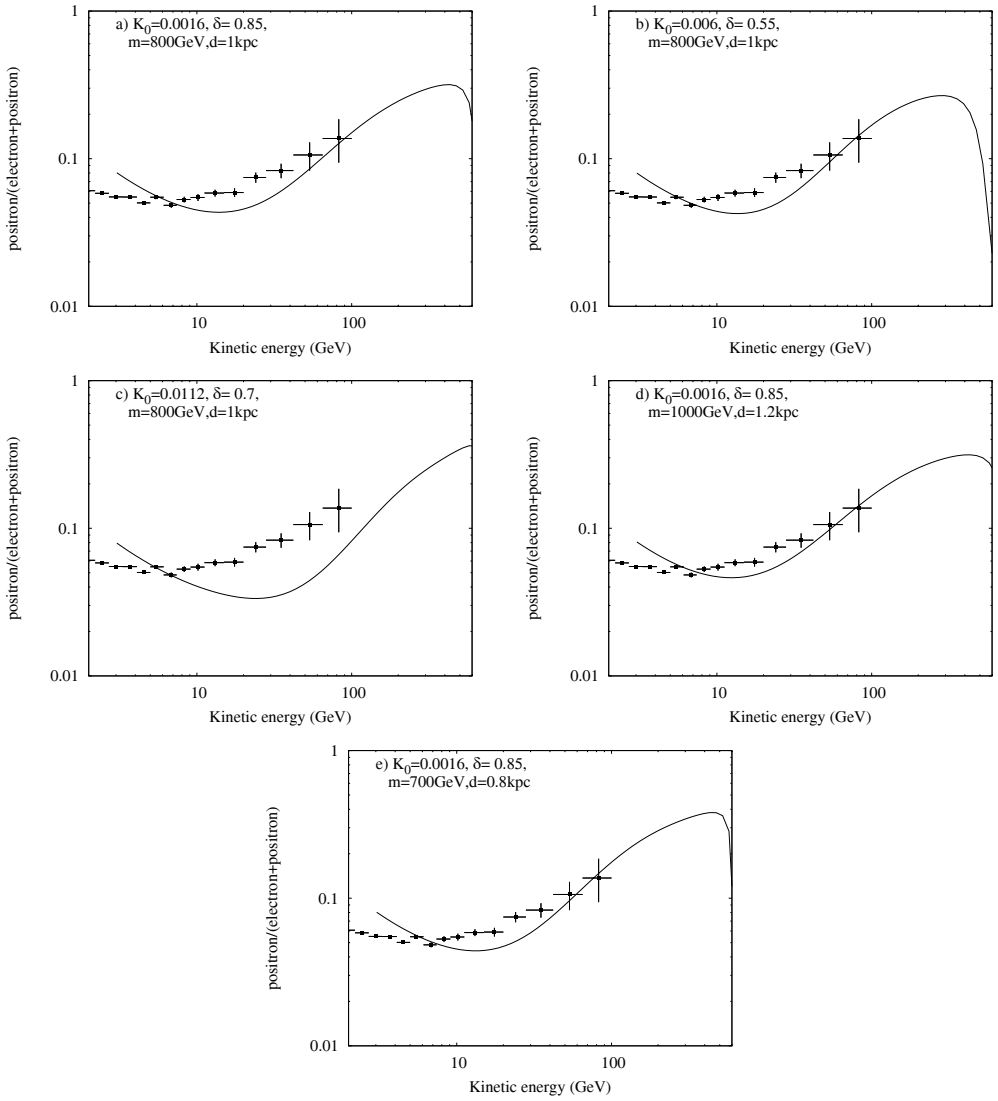

Fig. 1 Positron ratio from the IMBH boosted DM model. The curve is the positron ratio in our model, and the dots are the PAMELA data. The propagation parameters K_0 and δ, the DM mass m and the distance of the source to the solar system d are shown in each figure.

reduce the flux around the earth, setting an upper limit on the anti-proton flux if the convective current is ignored. Meanwhile, the convective current has little effect upon the high energy end, so the convective current and the continuous energy loss is omitted from the calculation. The propagation equation takes the form

$$-\nabla \cdot [K(\boldsymbol{x}, E)\nabla\varphi] + \Gamma(E)\varphi = q(\boldsymbol{x}, E), \tag{9}$$

where $\Gamma = \sigma v N$. N is the hydrogen atom number density in the disk. σ is the annihilation cross section between antiprotons and hydrogen atoms. v is the velocity of the antiproton. The propagation

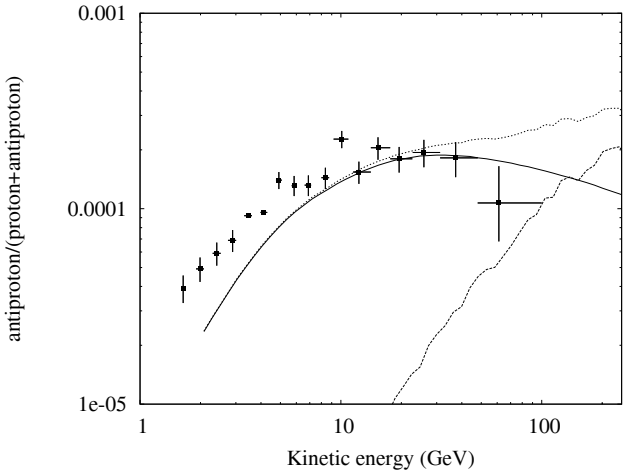

Fig. 2 Anti-proton results from a point source. The bottom dotted line is the point source result and the solid line is the classical result; the top dotted line is the total ratio including the classical and DM contributions. The dots are the PAMELA results.

equation is solved assuming a point source and the solution has the form

$$\varphi(E) = \frac{Q \cdot \exp\{-[\frac{\Gamma(E)}{K}] \cdot r\}}{4\pi K r}, \tag{10}$$

where φ is the flux. Precisely speaking, the solution to the propagation equation should take the boundary condition into account. However, the model we consider here is a nearby point source, which is far from the radial and z-axis boundary of the diffusion zone of the Galaxy and slightly affected by the boundary condition. Therefore, we take the spherical symmetry solution for the non-boundary space here. The result of the 800 GeV DM particle and point source at a distance of 1 kpc is shown in Figure 2. At 60 GeV, which is the central value of the highest energy point of PAMELA, the calculated anti-proton/proton ratio from DM annihilation is about a fifth of the value of the PAMELA data and the classical prediction. It is much less than the excess which is one order of magnitude higher. So, we can obtain the conclusion that, in our model, the antiproton from the DM annihilation is much smaller than the standard model prediction and contribution of this portion cannot be detected in the energy range of PAMELA. So, the PAMELA antiproton data is consistent with our model. However, for an even higher energy, the antiproton flux from DM annihilation is comparable to that predicted by the standard model, so an obvious excess of the ratio will show up. Further observations will test the model determinately.

4.3 Fitting the ATIC data

Setting $m = 800$ GeV and the source distance to be 1 kpc(a), $m = 700$ GeV; the source distance to be 0.8 kpc(b) and $m = 1000$ GeV; and the source distance to be 1.2 kpc(c), plotted together with the ATIC data, we obtain Figure 3.

The Q values are chosen to be the same as in the previous case where we fit the PAMELA data, i.e., 2×10^4 for 700 GeV, 3×10^4 for 800 GeV and 6×10^4 for 1000 GeV, respectively.

Some of the deviation may also result from the background spectrum we chose since it exists even at low energy. Regardless of these theoretical uncertainties, we can infer that for 800 GeV and

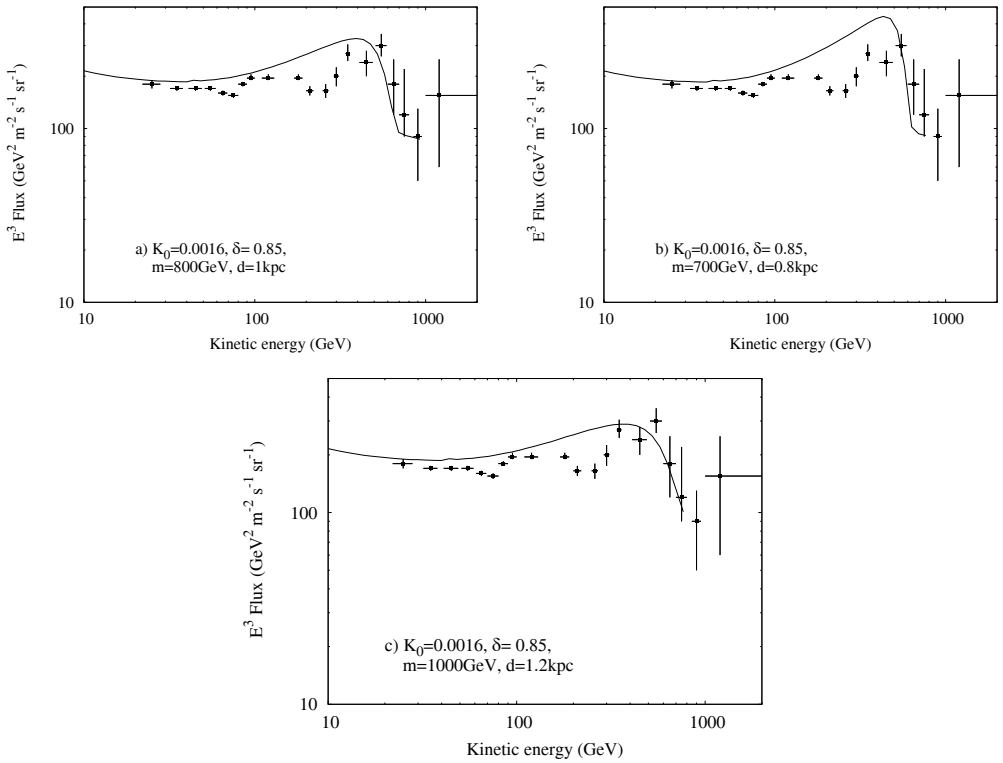

Fig. 3 Total electron+positron flux from the IMBH boosted DM model. The curve is the total flux in our model and the dots are the ATIC data. The propagation parameters K_0 and δ, the DM mass m and the distance of the source to the solar system d are shown in each figure.

1000 GeV DM particle mass, the result gives the same spectral shape as the ATIC data. We can see that the flux peaks at about 500 GeV and then there is a sharp decrease. The 700 GeV does not fit the ATIC result (Chang et al. 2008) well. At high energy, it gives too high an excess. This may be due to the smaller distance of the source. More high energy particles may survive in the propagation. We can infer that the distance of the source cannot be too small.

4.4 Pulsars

A pulsar could be another source of the positron excess (Hooper et al. 2009; Kobayashi et al. 2004). The strong magnetic field of pulsars can create high energy electron/positron pairs. Their spectrum has the form of

$$Q(E) \propto E^{-\gamma} \cdot \exp(-E/E_c), \tag{11}$$

where we choose $\gamma = 1.5$ and $E_c = 600$ GeV. The radiation energy of a pulsar attenuates quickly with time. Compared with the long electron/positron propagation time in the galaxy, the pulsar source can be treated as burst-like. The positron spectrum around the earth can be plotted by solving the propagation equation (Kobayashi et al. 2004). The spectrum depends not only on the total energy of the pulsar and the distance to earth, but also its age, owing to the short life time of the source. No mechanism exists for a pulsar to create high energy anti-protons, thus leaving no space for an excess of anti-protons. Pulsar results are shown in Figure 4 with two different parameter settings.

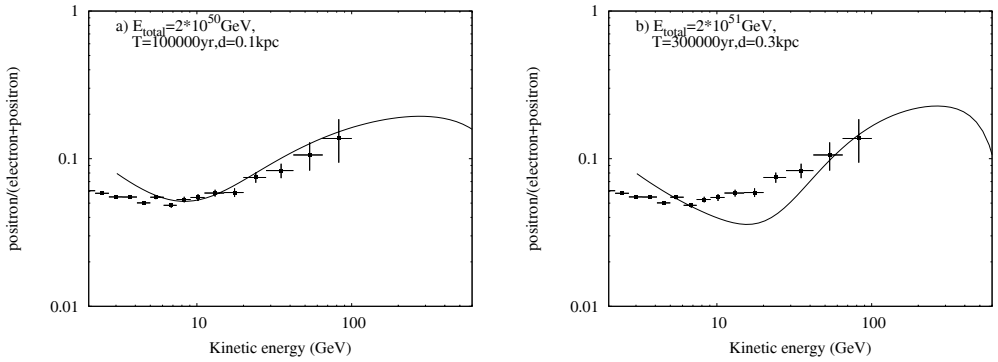

Fig. 4 Positron ratio produced by a pulsar *w*, compared with the PAMELA result. $E_{\rm total}$ is the energy radiated in the form of electron/positron pairs. T is the pulsar age and d is the distance of the pulsar.

From the figure, we find that a nearby pulsar (at 0.1 kpc, Fig. 4(a)) can fit the PAMELA data well, while a pulsar that is further away cannot give a good fit (Fig. 4(b)). However, there is a problem in the above calculation, where we take the total pulsar electron/positron energy to be the rather large value of about $10^{48} - 10^{49}$ erg, which is comparable to the total energy of a typical pulsar. Why so much energy is released in the form of electrons and positrons is a problem.

Acknowledgements We would like to thank X. L. Chen for valuable advice.

References

Adriani, O., Barbarino, G., Bazilevskaya, G., et al. 2009a, Nature, 458, 607
Adriani, O., Barbarino, G., Bazilevskaya, G., et al. 2009b, Phys. Rev. Lett., 102, 051101
Barrau, A., Salati, P., Servant, G., et al. 2005, Phys. Rev. D, 72, 063507
Bertone, G., Zentner, A., & Koushiappas, S. 2005, Phys. Rev. D, 72, 103517
Chang, J., Adams, J. H., Ahn, H. S., et al. 2008, Nature, 456, 362
Delahaye, T., Lineros, R., Donato, F., Fornengo, N., & Salati, P. 2008, Phys. Rev. D, 77, 063527
Donato, F., Maurin, D., Brun, P., et al. 2009, Phys. Rev. Lett., 102, 071301
Fornasa, M., & Bertone, G. 2008, Int. J. Mod. Phys. D, 17, 1125
Hooper, D., Blasi, P., & Serpico, P. 2009, J. Cosmol. Astropart. Phys., JCAP01(2009)025
Hooper, D., &Profumo, S. 2007, Phys. Rept., 453, 29
Kobayashi, T., Komori, Y., Yoshida, K., & Nishimura, J. 2004, ApJ, 601, 340
Maurin, D., Donato, F., Taillet, R., & Salati, P. 2001, ApJ, 555, 585
Moskalenko, I., & Strong, A. 1998, ApJ, 493, 694